Kinetic Studies of Ca^{2+} Binding and Ca^{2+} Clearance in the Cytosol of Adrenal Chromaffin Cells

Tao Xu,*# Mohammad Naraghi,* Huaguang Kang,# and Erwin Neher*
*Department of Membrane Biophysics, Max Planck Institute for Biophysical Chemistry, D-37077, Göttingen, Germany, and #Institute of Biophysics and Biochemistry, Huazhong University of Science and Technology, Wuhan 430074, China

ABSTRACT The Ca^{2+} binding kinetics of fura-2, DM-nitrophen, and the endogenous Ca^{2+} buffer, which determine the time course of Ca^{2+} changes after photolysis of DM-nitrophen, were studied in bovine chromaffin cells. The in vivo Ca^{2+} association rate constants of fura-2, DM-nitrophen, and the endogenous Ca^{2+} buffer were measured to be 5.17×10^8 M^{-1} s^{-1}, 3.5×10^7 M^{-1} s^{-1}, and 1.07×10^8 M^{-1} s^{-1}, respectively. The endogenous Ca^{2+} buffer appeared to have a low affinity for Ca^{2+} with a dissociation constant around 100 μM. A fast Ca^{2+} uptake mechanism was also found to play a dominant role in the clearance of Ca^{2+} after flashes at high intracellular free Ca^{2+} concentrations ($[Ca^{2+}]_i$), causing a fast $[Ca^{2+}]_i$ decay within seconds. This Ca^{2+} clearance was identified as mitochondrial Ca^{2+} uptake. Its uptake kinetics were studied by analyzing the Ca^{2+} decay at high $[Ca^{2+}]_i$ after flash photolysis of DM-nitrophen. The capacity of the mitochondrial uptake corresponds to a total cytosolic Ca^{2+} load of ~1 mM.

INTRODUCTION

Intracellular free Ca^{2+} plays a crucial role as a second messenger in the control of secretion, metabolic activities, muscle contraction, and gene expression. The photolabile calcium chelator DM-nitrophen (DMN) has been used extensively to study calcium-triggered exocytosis (Kaplan and Ellis-Davies, 1988; Neher and Zucker, 1993; Thomas et al., 1993; Heidelberger et al., 1994). Because the rate of exocytosis depends steeply on the intracellular free Ca^{2+} concentration ($[Ca^{2+}]_i$), it is important to have a better understanding of $[Ca^{2+}]_i$ dynamics generated by photolysis of DMN in cells. The time course of $[Ca^{2+}]_i$ after flash photolysis is determined by the Ca^{2+} binding kinetics of Ca^{2+} indicator dyes, DMN, other added exogenous or the endogenous Ca^{2+} buffers, as well as the Ca^{2+} clearance mechanisms in the cell. A question of particular interest is whether large Ca^{2+} spikes exist during flashes, which are invisible to the common $[Ca^{2+}]_i$ fluorescence measurement but may significantly accelerate secretion. Furthermore, it is important to know how much DMN is required for maintaining $[Ca^{2+}]_i$ at a constant level after flashes.

Zucker (1993) showed that in vitro flashes of DMN could generate a large (tens to hundreds of μM) transient increase in $[Ca^{2+}]_i$ milliseconds in duration. But by monitoring the capacitance change after flashes, Neher and Zucker (1993) and Heinemann et al. (1994) did not observe indirect indications of such $[Ca^{2+}]_i$ spikes. One of the explanations Heinemann et al. offered for their findings was the existence of a fast endogenous Ca^{2+} buffer at a sufficiently high concentration to attenuate the $[Ca^{2+}]_i$ spikes. Moreover, in some studies, the $[Ca^{2+}]_i$ after flashes decayed slowly, lasting tens of seconds, whereas Gillis et al. (1996) observed a fast decay, with a time constant of 1 s, when MgATP was present in the pipette. These findings raise the question of whether this fast decay is due to a complex interaction between DMN, Ca^{2+}, and Mg^{2+} that takes place in ATP-containing solutions, or is a consequence of bioenergetic mechanisms.

Although some in vitro kinetic studies on Ca^{2+} indicator dyes and DMN have been reported (Kao and Tsien, 1988; Zucker, 1993; Ellis-Davies et al., 1996; Escobar et al., 1995), little is known about the Ca^{2+} binding kinetics of these compounds in vivo. In a previous study on bovine chromaffin cells, Zhou and Neher (1993) found a mostly immobile endogenous Ca^{2+} buffer with a Ca^{2+} binding ratio of 40. The Ca^{2+} affinity of this endogenous Ca^{2+} buffer was assumed to be low because its binding ratio was not reduced by elevating basal $[Ca^{2+}]_i$ to even 3 μM. To understand the role of cellular Ca^{2+} buffers in shaping the high-level Ca^{2+} signals, we must have more precise information about their Ca^{2+} dissociation constants (K_d) and their on rates of Ca^{2+} binding.

Mitochondria are known to play a dominant role in the clearance of large Ca^{2+} loads from the cytosol (Nicholls and Åkermann, 1982). Recent studies by Herrington et al. (1996) and Park et al. (1996) suggest that this is relevant for rat adrenal chromaffin cells. Because this Ca^{2+} uptake is apparently activated cooperatively at elevated $[Ca^{2+}]_i$, it may not be negligible in sequestering Ca^{2+} when $[Ca^{2+}]_i$ reaches levels as high as tens of μM after flash photolysis, although previous investigations in bovine chromaffin cells at lower $[Ca^{2+}]_i$ did not point to such a mechanism. Thus it must be clarified whether mitochondrial uptake or other Ca^{2+} clearance mechanisms play a significant role in shaping the $[Ca^{2+}]_i$ after flash photolysis in bovine chromaffin cells.

Received for publication 30 October 1996 in final form 12 April 1997.

Address reprint requests to Dr. Erwin Neher, Abteilung Membranbiophysik, Max-Planck-Institut für Biophysikalische Chemie, Am Fassberg, D-37077 Gottingen, Germany. Tel.: +49-551-201-1630; Fax: +49-551-201-1688; E-mail: eneher@gwdg.de.

0006-3495/97/07/532/14 $2.00

In this study, we applied flash and steady-state UV photolysis of DMN to quantitatively release Ca^{2+} in bovine chromaffin cells. We studied the kinetics of Ca^{2+} binding to fura-2, DMN, and an "endogenous Ca^{2+} buffer" by monitoring the relaxation of the fluorescence signal of Ca^{2+} indicators. In our definition of "endogenous Ca^{2+} buffer," we lump together all cellular Ca^{2+} buffers that are in rapid equilibrium with free calcium and remain in the cell after minutes of whole-cell recording. In addition, a fast Ca^{2+} uptake by mitochondria activated in a high range of $[Ca^{2+}]_i$, causing $[Ca^{2+}]_i$ to decay within seconds, was identified and studied.

MATERIALS AND METHODS

Cell preparation and patch-clamp experiments

Chromaffin cells from bovine adrenal glands were prepared and cultured as described by Zhou and Neher (1993). Cells were used 1–4 days after preparation. The external bathing solution for experiments contained 150 mM NaCl, 2.8 mM KCl, 2 mM $CaCl_2$, 1 mM $MgCl_2$, 10 mM HEPES, and 2 mg/ml glucose (pH 7.2, 320 mosm). In some experiments, $CaCl_2$ was omitted to minimize the Ca^{2+} influx. For preparing pipette solutions, we generally used 2× the concentrated buffer, which contained 290 mM Cs-glutamate, 40 mM HEPES, 12 mM NaCl (pH 7.2). We added different concentrations of DMN, fura-2, furaptra, $CaCl_2$, ATP, etc. (see Table 1), for different purposes, as indicated in the text. The resulting mixtures were diluted with double-distilled water for the appropriate osmolarity (310 mosm). The pipette solution was adjusted to pH 7.2 by either HCl or CsOH. Typical compositions of pipette solutions are shown in Table 1. Conventional whole-cell recording (Hamill et al., 1981) was performed with 2–4-MΩ pipettes. The membrane potential was held at −70 mV. All experiments were performed at room temperature.

All reagents were from Sigma (St. Louis, MO), except as otherwise noted. Carbonyl cyanide *m*-chlorophenylhydrazone (CCCP) was prepared as a stock solution at a concentration of 10 mM in dimethyl sulfoxide (DMSO). The final concentration of DMSO in diluted solution was 0.02%.

Photolysis of caged Ca^{2+} and $[Ca^{2+}]_i$ measurement

Flashes of UV light and fluorescence excitation light were produced as described by Heinemann et al. (1994) and coupled to the epiillumination port of a Zeiss IM35 inverted microscope with a 100× oil immersion objective (NA 1.3). Rectangular field stops were used to restrict illumination to a square area of 40 × 40 μm. The cell under study was located in the center of this illuminated area. Fluorescence from a circular subarea of 20 μm diameter that contained the cell was measured with a photomultiplier tube (PMT) (Hamamatsu R928 coupled to a photometer S; Zeiss). For fast kinetic measurements, the cutoff frequency of the photometer was set to >5000 Hz, thus allowing the measurement of millisecond fluorescence relaxations. The detection light path contained a 470-nm long-pass filter and a 540-nm short-pass filter.

We used a UV flash lamp (Rapp Optoelektronik, Hamburg, Germany) and a polychromatic light source (T.I.L.L. Photonics GmbH, Gräfelfing, Germany). The latter served as a steady-state UV light source to photolyze DMN tetrasodium salt (Calbiochem, La Jolla, CA). The photolysis efficiency of the flash lamp was first determined as described by Heinemann et al. (1994), however, using whole-cell dialysis instead of droplets in octanol. The method for measuring the flash photolysis efficiency was later refined in the following way: we used high concentrations of fura-2 (500 μM to 1 mM) to overcome the endogenous Ca^{2+} buffer, and used fully loaded DMN in the absence of MgATP during flash experiments. Small flash intensities were applied by adding neutral density (ND) filters. We verified that the calibration constants for fura-2 measurement were not significantly altered before and after flashes by using small flash intensities and hence small degrees of photolysis. From measurements of $[Ca^{2+}]_i$ before and immediately after flashes, we calculated the photolysis efficiency for Ca-bound DMN. In these experiments, $[Ca^{2+}]_i$ typically rose from several tens of nM before flashes to hundreds of nM after flashes, under which conditions the mitochondrial Ca^{2+} uptake would not be activated (Herrington et al., 1996; Park et al., 1996). Knowing the Ca^{2+} binding ratio of fura-2 and assuming that all Ca^{2+} liberated by DMN binds to fura-2 or appears as free Ca^{2+}, we determined the photolysis efficiency of a 300-V discharge flash with 10% ND filters for Ca-bound DMN to be 13.4%.

Because the fluorescence excitation wavelength also covers the UV range that can photolyze DMN, we can use the fluorescence excitation light to measure $[Ca^{2+}]_i$ and photorelease Ca^{2+} simultaneously. The rate of photolysis of fluorescence excitation light was determined in the following manner. We used fully loaded DMN (0.5 mM) and a high concentration of fura-2 (1–2 mM), so that fura-2 was the dominant Ca^{2+} buffer and the dominant fluorophore, overcoming the fluorescence of DMN and its photoproducts. Under these conditions all Ca^{2+} molecules released from DMN would be taken up by fura-2. Let R_p denote the rate of photolysis of Ca-bound DMN (CaN) while the steady-state UV light is on. CaN and the increase in Ca-bound fura-2 (ΔCaF) will satisfy the following equations:

$$[\mathrm{CaN}]_t = [\mathrm{N}]_{T,0} \cdot e^{-R_p \cdot t} \quad (1)$$

$$\Delta[\mathrm{CaF}]_t \approx [\mathrm{N}]_{T,0} \cdot (1 - e^{-R_p \cdot t}) \quad (2)$$

where t is the time and $[N]_{T,0}$ is the initial total concentration of DMN. By fitting the fluorescence signal sampled during steady-state photolysis of DMN, one can get the exact R_p value. The basis for this method (used for the measurement as described below) relies on the high Ca^{2+} affinity of DMN in the absence of magnesium. The K_d (Ca^{2+}) of DMN under these conditions was measured to be 5 nM, meaning that more than 95% of DMN molecules are in the Ca^{2+}-bound state at $[Ca^{2+}]_i > 100$ nM. The R_p for 380 nm and 390 nm excitation wavelength in our setup was found by this method to be 1.497 ± 0.005 s^{-1} and 0.966 ± 0.050 s^{-1} (mean ± SD), respectively.

The calibration constants for fura-2 (Grynkiewiez et al., 1985) and furaptra (Konishi et al., 1991) measurements before and after 300-V discharge flashes were measured by dialyzing cells with zero (R_{min}), intermediate (K_{eff}), and high (R_{max}) Ca^{2+} concentrations as described by Neher (1989) and Heinemann et al. (1994). For pipette solutions containing 1.0 mM DMN and 50 μM fura-2 (lot 509; Texas Fluorescence Labs, Austin, TX), the changes in the calibration constants (dual wavelength measurement at 340 and 390 nm) by a 300-V discharge flash were as follows: R_{min} changed from 0.304 to 0.355, R_{max} from 15.76 to 13.81, K_{eff} from 3968 nM to 5298 nM. Calibration constants for different flash intensities between 0 and 100% at 300-V discharge, with different ND filters, were estimated by linear interpolation of the above values. For furaptra measurements, 40 mM 1,3-diaminopropane-2-ol-*N*,*N*′-tetraacetic acid (DPTA) was used to overcome the endogenous Ca^{2+} buffer and to buffer the $[Ca^{2+}]_i$ to an intermediate level. For 5 mM DMN, 0.2 mM

TABLE 1 Solutions used for experiments

	A	B	C	D	E
Na_4-DMN	1	10.9	4	5	10
Cs-glutamate	145	116	130	130	101
Cs-HEPES	20	16	18	18	14
NaCl	6	4.8	5.4	5.4	4.2
$CaCl_2$	1	5	4	4.8	9.6
Na_2ATP	—	—	—	—	2
Fura-2	0.05	0.2	2	—	—
Furaptra	—	—	—	0.2	1

All concentrations are millimolar (mM).

furaptra (Molecular Probes, Eugene, OR), the changes in the calibration constants (alternating at 340 and 380 nm) were as follows: R_{min} changed from 0.194 to 0.201, R_{max} from 4.935 to 4.581, and K_{eff} from 1866 μM to 2606 μM.

$[Ca^{2+}]_i$ was calculated from the fluorescence ratio R according to the method of Grynkiewiez et al. (1985):

$$[Ca^{2+}]_i = K_{eff}\frac{R - R_{min}}{R_{max} - R} \tag{3}$$

In the case of single wavelength $[Ca^{2+}]_i$ measurements, if the prestimulus fluorescence, $F(0)$, was not at its maximum value (F_{max}, obtained at low $[Ca^{2+}]_i$ when measured at 380 nm), the following expressions from Neher and Augustine (1992)

$$\gamma = \frac{F(t)}{F(0)}\cdot\frac{K_{eff} + [Ca^{2+}]_{i,0}}{K_d + [Ca^{2+}]_{i,0}} \tag{4}$$

$$[Ca^{2+}]_{i,t} = \frac{K_{eff} - \gamma\cdot K_d}{\gamma - 1} \tag{5}$$

were used, where $[Ca^{2+}]_{i,0}$ was the initial (resting) value of $[Ca^{2+}]_i$, determined by Eq. 3. If $F(0)$ was approximately F_{max} (see results), the single-wavelength fluorescent signals $F(t)$ were divided by $F(0)$, which gave $F' = F(t)/F(0)$, and $[Ca^{2+}]_i$ was calculated by

$$[Ca^{2+}]_i = K_d\cdot\frac{1 - F'}{F' - F_{min}/F_{max}} \tag{6}$$

Notations and equations

The notations used in this paper and their definitions are shown in Table 2.

Fluorescence relaxation measurements made by flash photolysis

Given the following system:

$$Ca^{2+} + X \underset{\beta_X}{\overset{\alpha_X}{\rightleftarrows}} CaX \tag{7}$$

$$Ca^{2+} + F \underset{\beta_F}{\overset{\alpha_F}{\rightleftarrows}} CaF \tag{8}$$

where X can be any Ca^{2+} chelator and F is the fluorescent Ca^{2+} indicator fura-2. When total Ca^{2+} is incremented in a steplike fashion, e.g. by flash photolysis of DMN, the system will be perturbed and reach a new equilibrium state. For small perturbations, relaxations of [CaF] with rate λ given by

$$\lambda = \frac{\lambda_X + \lambda_F - \sqrt{(\lambda_X + \lambda_F)^2 - 4\cdot\alpha_F\cdot\{\lambda_X\cdot(K_{d,F} + \overline{[Ca^{2+}]_i}) + \alpha_X\cdot\overline{[F]}\cdot(K_{d,X} + \overline{[Ca^{2+}]_i})\}}}{2} \tag{9}$$

will be observed, where

$$\lambda_X = \alpha_X\cdot(\overline{[X]} + \overline{[Ca^{2+}]_i}) + \beta_X \tag{10}$$

$$\lambda_F = \alpha_F\cdot(\overline{[F]} + \overline{[Ca^{2+}]_i}) + \beta_F \tag{11}$$

Bars above concentration symbols signify that the concentration at the new equilibrium state was used. According to Grynkiewiez et al. (1985),

$$\begin{aligned} F_2(t) &= S_{f2}\cdot[F] + S_{b2}\cdot[CaF] \\ &= S_{f2}\cdot[F]_T + (S_{b2} - S_{f2})\cdot[CaF] \end{aligned} \tag{12}$$

which means [CaF] is a linear function of the Ca^{2+}-sensitive fluorescence. Thus, by measuring the relaxation of average cellular fluorescence, we can get the on rate and off rate of Ca^{2+} binding to chelator X, provided its dissociation constant, α_F, and β_F of fluorescent dye are known.

Kinetic measurements with steady-state UV illumination

For slow Ca^{2+} chelators such as DMN, we can measure its Ca^{2+} binding rate by using steady-state UV photolysis. In the case of three Ca^{2+} chelators, F, E, and N, the rate of $[Ca^{2+}]_i$ change will satisfy the following equation:

$$\frac{d[Ca^{2+}]_i}{dt} = R_p\cdot[CaN] - \frac{d[CaN]}{dt} - \frac{d[CaF]}{dt} - \frac{d[CaE]}{dt} \tag{13}$$

If DMN has a much greater binding ratio than fura-2 and the endogenous Ca^{2+} buffer, then, once the steady-state UV light is on, the Ca^{2+} being liberated will almost completely rebind to unphotolyzed DMN. Hence a balance between releasing from and rebinding to DMN will be established. Because the rebinding rate is determined by the Ca^{2+} on rate, we can then measure the on rate of DMN if the releasing rate is known. In fact, let κ_F and κ_E be the binding ratios of fura-2 and the endogenous Ca^{2+} buffer, respectively. We have

$$\frac{d[CaF]}{dt} = \kappa_F\cdot\frac{d[Ca^{2+}]_i}{dt}, \quad \frac{d[CaE]}{dt} = \kappa_E\cdot\frac{d[Ca^{2+}]_i}{dt}$$

and

$$\begin{aligned} (1 + \kappa_F + \kappa_E)\cdot\frac{d[Ca^{2+}]_i}{dt} &= R_p\cdot[CaN] - \frac{d[CaN]}{dt} \\ &= R_p\cdot[CaN] - \alpha_N\cdot([Ca^{2+}]_i\cdot[N] - K_{d,N}\cdot[CaN]) \end{aligned} \tag{14}$$

where the binding ratio of X is calculated according to the method of Zhou and Neher (1993) as

$$\kappa_X = \frac{[X]_T\cdot K_{d,X}}{([Ca^{2+}]_i + K_{d,X})^2} \tag{15}$$

α_N can be solved from Eq. 14 as

$$\alpha_N = \frac{R_p\cdot[CaN] - (1 + \kappa_F + \kappa_E)\cdot(d[Ca^{2+}]_i/dt)}{[Ca^{2+}]_i\cdot[N] - K_{d,N}\cdot[CaN]} \tag{16}$$

TABLE 2 Notations and definitions

Notation	Definition
F, Fp, E, N, P	fura-2, furaptra, endogenous Ca^{2+} buffer, DMN and photoproducts of DMN
α_X	Ca^{2+} binding rate of X (X = F, E, N)
β_X	Ca^{2+} dissociation rate of X (X = F, E, N)
$K_{d,X}$	Ca^{2+} dissociation constant of X (X = F, Fp, E, N, P)
CaX	Ca-bound form of X (X = F, Fp, E, N, P)
$[X]_T$	Total concentration of X ($[X]_T$ = [CaX] + [X])
K	Ratio of quantum efficiency between Ca-bound DMN and free DMN (K = 2.5, according to Zucker, 1993)
R_p	Rate of photolysis of Ca-bound DMN by steady UV light

As long as $[N]_{T,t}$ is in excess of total Ca ($[Ca]_T$), nearly all of the Ca^{2+} will bind to DMN, thus [CaN] = $[Ca]_T$, [N] = $[N]_{T,t}$ − [CaN]. According to equation 6 of Zucker (1993), $[N]_{T,t}$ can be calculated as

$$[N]_{T,t} = \{[N]_{T,0} - (1 - K)\cdot[Ca]_T\}\cdot e^{-R_p\cdot t/K} + (1 - K)\cdot[Ca]_T \quad (17)$$

$[Ca^{2+}]_i$ and $d[Ca^{2+}]_i/dt$ can be measured from the fluorescent signal. If R_p is known, we can then obtain α_N from Eq. 16.

Kinetic measurement of mitochondrial Ca^{2+} uptake

The Ca^{2+} uptake rate (J) of mitochondria was assumed to follow a second-order Hill equation according to Gunter et al. (1994):

$$J([Ca^{2+}]_i) = \frac{V_{max}\cdot[Ca^{2+}]_i^2}{K_{1/2}^2 + [Ca^{2+}]_i^2} \quad (18)$$

If mitochondrial Ca^{2+} uptake dominates Ca^{2+} clearance in the first second after flashes that elevate $[Ca^{2+}]_i$ to levels greater than 10 μM, the kinetics of $[Ca^{2+}]_i$ changes can be described as

$$(1 + \kappa_E + \kappa_F + \kappa_A)\cdot\frac{d[Ca^{2+}]_i}{dt} = -J([Ca^{2+}]_i) \quad (19)$$

where κ_E, κ_F, and κ_A are the binding ratios of the endogenous Ca^{2+} buffer, Ca^{2+} indicator, and other added Ca^{2+} buffers, respectively. Assuming that κ_E, κ_F, and κ_A are relatively constant during small $[Ca^{2+}]_i$ changes, Eqs. 18 and 19 can be solved to yield the following:

$$\frac{[Ca^{2+}]_i^2 - K_{1/2}^2}{[Ca^{2+}]_i} = \frac{[Ca^{2+}]_{i,0}^2 - K_{1/2}^2}{[Ca^{2+}]_{i,0}} - \frac{V_{max}}{1 + \kappa_E + \kappa_F + \kappa_A}\cdot t \quad (20)$$

where $[Ca^{2+}]_{i,0}$ is the $[Ca^{2+}]_i$ level immediately after the flash. In the extreme case where $[Ca^{2+}]_i^2 \gg K_{1/2}^2$, we can simplify Eq. 20 to

$$[Ca^{2+}]_i = [Ca^{2+}]_{i,0} - \frac{V_{max}}{1 + \kappa_E + \kappa_F + \kappa_A}\cdot t \quad (21)$$

which means $[Ca^{2+}]_i$ will decline as a linear function with a slope of $V_{max}/(1 + \kappa_E + \kappa_F + \kappa_A)$. By linear fitting of the initial $[Ca^{2+}]_i$ decay rate and knowing the Ca^{2+} binding ratio of all cytosolic buffers, we can then measure the V_{max}. Considering another extreme case where $[Ca^{2+}]_i^2 \ll K_{1/2}^2$, Eq. 20 can be simplified to

$$\frac{1}{[Ca^{2+}]_i} = \frac{1}{[Ca^{2+}]_{i,0}} + \frac{V_{max}}{(1 + \kappa_E + \kappa_F + \kappa_A)\cdot K_{1/2}^2}\cdot t \quad (22)$$

which means one can obtain the value of $K_{1/2}$ by measuring the rate of change of the reciprocal of $[Ca^{2+}]_i$ after the flash.

The amount of Ca^{2+} that is accumulated by mitochondria can be calculated by

$$\int_0^t J([Ca^{2+}]_i)\cdot dt = [Ca]_{T,0} - [Ca]_{T,t} \quad (23)$$

where

$$[Ca]_{T,t} = [Ca^{2+}]_i + \sum_X \frac{[Ca^{2+}]_i\cdot[X]_T}{[Ca^{2+}]_i + K_{d,X}} \quad (24)$$

and the sum extends over all cytosolic buffers. If the capacity of mitochondrial Ca^{2+} uptake is nonsaturable, which means Eq. 18 will be valid for calculating the Ca^{2+} influx rate during the entire experiment, then the Ca^{2+} accumulated in mitochondria can be estimated just by integrating Eq. 18 over time. Any deviations between the experimental measurement of the total amount of Ca^{2+} influx into mitochondria according to Eq. 23 and those from integration of Eq. 18 (using measured values of V_{max} and $K_{1/2}$) can be taken as an indication that mitochondrial uptake reaches its maximum capacity. Therefore, such deviations provide insight into the capacity of mitochondrial Ca^{2+} uptake in living cells.

Analysis

The fittings and simulations were conducted on a Macintosh computer using IGOR Pro (WaveMetrics, Lake Oswego, OR). For simulations, the first-order differential equations derived from the reaction scheme were solved numerically by first-order Euler integration. All of the fittings were done by using the intrinsic fitting functions of IGOR.

RESULTS

Our goal is to measure the kinetics of Ca^{2+} binding to Ca^{2+} chelators and Ca^{2+} clearance in the cytosol. For fast kinetic studies, the most common method is to measure the relaxations while shifting the reaction system from one equilibrium state to another equilibrium. This, then, requires at least three Ca^{2+} chelators to be present in the cytosol. One is the inevitable endogenous Ca^{2+} buffer, the second one must be the Ca^{2+} source (such as DMN) for releasing Ca^{2+} as a perturbation, and the third one is the Ca^{2+} indicator for reporting the relaxations. In general, it is hard to solve the Ca^{2+} chelating reaction system with three nonlinear differential equations. But as shown below, by carefully designing the experimental conditions, one can simplify the kinetic system and dissect both kinetic and steady-state properties of different Ca^{2+} chelators.

Ca^{2+} binding kinetics of fura-2 in vivo

DMN has a very high affinity for Ca^{2+} and relatively slow Ca^{2+} binding kinetics as compared with fura-2 and the endogenous Ca^{2+} buffer. Thus we filled the pipette with solution A (Table 1) for measuring the Ca^{2+} binding kinetics of fura-2. The solution was designed to fully load DMN with Ca^{2+}. The basal $[Ca^{2+}]_i$ levels were around several hundreds of nM, as measured by fura-2. DMN would then not act as a chelator, but only serve as a Ca^{2+} source for fast release of Ca^{2+}. Because most of the Ca^{2+} that was released from DMN would bind to fura-2 and the endogenous Ca^{2+} buffer, we could use Scheme 7 and Scheme 8 to describe the kinetic system of Ca^{2+} chelating, where X represented the endogenous Ca^{2+} buffer (E).

From Zhou and Neher (1993), we know that the Ca^{2+} buffer in bovine chromaffin cell has a low affinity ($K_{d,E} >$ 10 μM) and a total concentration of more than 0.4 mM. Also by considering that [F] is low in solution A and that most Ca^{2+}-binding proteins in cells have on rates of $\sim 10^8$ $M^{-1}\,s^{-1}$ (Falke et al., 1994), we have $\lambda_E \gg \lambda_F$ if $[Ca^{2+}]_i >$ 1 μM, according to Eqs. 10 and 11. Under this condition,

$[Ca^{2+}]_i$ will undergo a steplike fast change, and Eq. 9 simplifies to

$$\lambda = \alpha_F \cdot \overline{[Ca^{2+}]_i} + \beta_F \quad (25)$$

The relaxation rate λ of the fura-2 fluorescence is a linear function of equilibrium $[Ca^{2+}]_i$. Three fluorescence relaxation traces after UV flashes are shown in Fig. 1 *A*. It is seen that relaxation is faster with higher $[Ca^{2+}]_i$. In Fig. 1 *B*, we present fitted relaxation rates against $[Ca^{2+}]_i$ measured according to Eq. 5. The data are pooled from 47 cells because of a relatively low signal-to-noise ratio due to a high cutoff frequency of the PMT and a small concentration of fura-2. A linear relationship between the fura-2 relaxation rate ($\lambda_{fura\text{-}2}$) and $[Ca^{2+}]_i$ is apparant. By linear fitting of Fig. 1 *B* in the $[Ca^{2+}]_i$ range of 1–3 μM while constraining $K_{d,F}$ to 231.8 nM (a value calculated from our calibration constants and the measurement of the isocoefficient according to equation 2 of Zhou and Neher, 1993), we get an on rate of $5.17 \times 10^8\ M^{-1}\ s^{-1}$ for fura-2. The data are also fitted with Eq. 9, where $K_{d,E}$ and $[E]_T$ are assumed to be 100 μM and 4 mM, respectively (see below). This results in almost the same α_F of $4.98 \times 10^8\ M^{-1}\ s^{-1}$. From the on rate and $K_{d,F}$ one can calculate an off rate of 119.4 s^{-1} for fura-2.

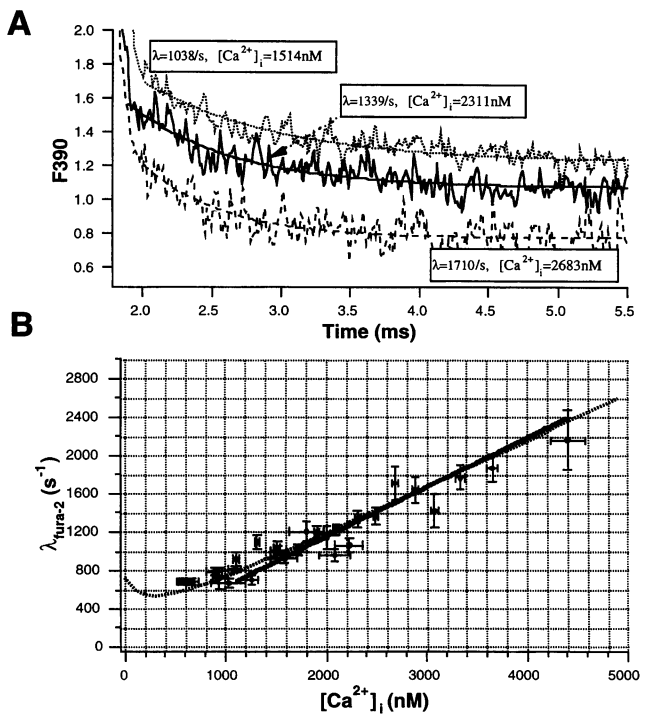

FIGURE 1 Ca^{2+} binding kinetics of fura-2. The pipette solution was solution A (Table 1). (*A*) Relaxations of three fluorescence traces exited at 390 nm. At zero time, a flash was triggered. We verified that there was no artifact at 2 ms after the flash light had decayed. The 390-nm excitation light was also turned on at zero time because the adjustment of the wavelength takes 2 ms by our polychromator. The smooth lines represent single exponential fits to the fluorescence signal. The concentrations of equilibrium $[Ca^{2+}]_i$ as well as the fitted relaxation rates are indicated for individual traces. (*B*) Relaxation rates versus $[Ca^{2+}]_i$. Pooled averages of relaxation rates (●) from 47 cells are plotted against $[Ca^{2+}]_i$. Traces with similar $[Ca^{2+}]_i$ levels were averaged and fitted by single exponential functions to obtain relaxation rates. The error bar for rates represents confidence limits given by the fitting program. For $[Ca^{2+}]_i$ the error bar represents the standard deviation. ——, a line fit; – – –, a fit with Eq. 9.

Ca^{2+} binding kinetics of DMN in vivo

Based on the relatively slow kinetics of DMN, we can slowly release Ca^{2+} by steady UV photolysis to measure the Ca^{2+} binding kinetics of DMN. The idea is that nearly all of the Ca^{2+} that is slowly being released by photolysis will rebind to unphotolyzed DMN if DMN is the dominant Ca^{2+} chelator (by partially loading DMN). Because the rebinding rate is proportional to the product of $[Ca^{2+}]_i$ and the Ca^{2+} on rate of DMN, we can calculate the Ca^{2+} on rate of DMN once $[Ca^{2+}]_i$ is known. Alternatively, we can measure the kinetics of DMN by adjusting the Ca^{2+}-buffering capacity of DMN and fura-2 significantly above that of the endogenous Ca^{2+} buffer. Thus the impact of the endogenous Ca^{2+} buffer is negligible. By measuring the fluorescence relaxation rates after fast flash photorelease of Ca^{2+} and applying Eq. 9, we are able to find the Ca^{2+} on rate of DMN. In the following, we describe the measurement of the Ca^{2+} on rate of DMN, using both steady UV photolysis and flash photolysis.

Fig. 2 *A* displays seven normalized fura-2 fluorescence traces in response to steady 380-nm photolysis starting at time 0. The traces from seven different cells are virtually superimposable, demonstrating the reproducibility of the time course. The pipette solution was solution B (Table 1). In each case, 380-nm UV light was turned on after an equilibrium between pipette and cytosol was established. Fig. 2 *A* shows a fast decay in fluorescence followed by a plateau of several hundred milliseconds' duration, which represents the establishment of a balance between the release of Ca^{2+} by photolysis and the rebinding of Ca^{2+} to unphotolyzed DMN. Then, as unphotolyzed DMN diminishes, the fluorescence drops faster again while fura-2 approaches saturation. At the beginning of the trace, DMN is 46% loaded and the basal $[Ca^{2+}]_i$ is clamped to 4 nM. Under this condition, 98.3% of the fura-2 is in its free form. This means that $F(0)$ is close to F_{max} excited at 380 nm. $[Ca^{2+}]_i$ is then calculated according to Eq. 6 (plotted in Fig. 2 *B*). The rate of $[Ca^{2+}]_i$ change ($d[Ca^{2+}]_i/dt$) during a 0.1–0.3-s time window is estimated to be 208 nM/s; thus the term $(1 + \kappa_F + \kappa_E) \cdot d[Ca^{2+}]_i/dt$ in Eq. 16 is 140 μM/s in this case. This is negligible compared to the term $R_p \cdot [CaN]$, which is 7.5 mM/s. The average of on rates of DMN was calculated to be $3.41 \pm 0.23 \times 10^7\ M^{-1}\ s^{-1}$ ($n = 7$) for 380-nm illumination and $3.58 \pm 0.3 \times 10^7\ M^{-1}\ s^{-1}$ ($n = 7$) for 390-nm illumination (mean ± SD). The results of computer simulations solving a system of kinetic equations that represent the same condition (Eq. 14) are also plotted in Fig. 2 *B*. The measured $[Ca^{2+}]_i$ can best be fitted by assuming an α_N of $3.2 \times 10^7\ M^{-1}\ s^{-1}$, except for an initial rising phase. Here the slow kinetics of fura-2 and the

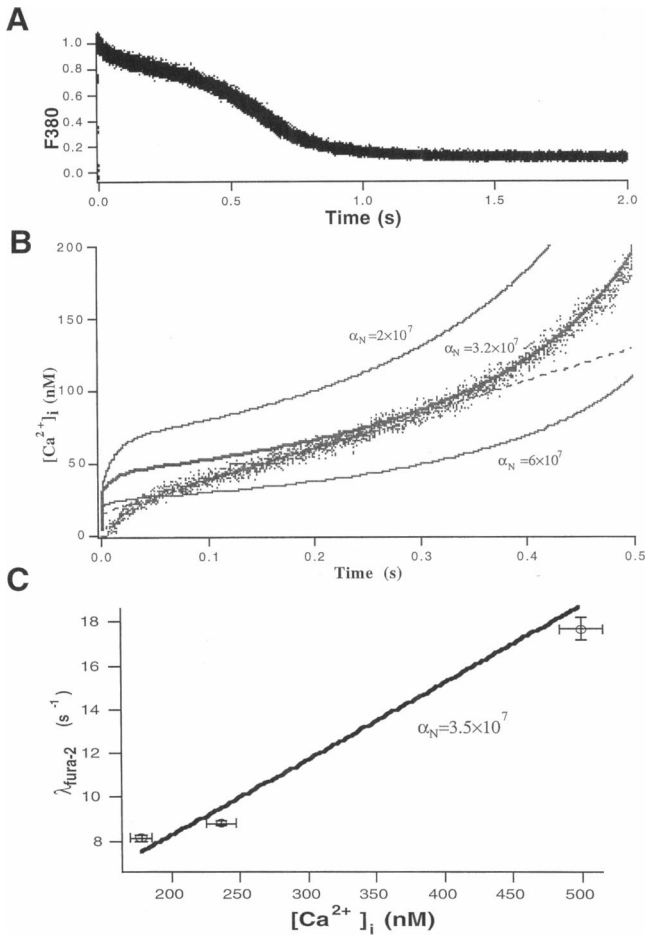

FIGURE 2 Ca^{2+} binding kinetics of DMN. The Ca^{2+} on rate of DMN was studied either by steady-state UV photolysis (*A*, *B*) or by flash photolysis (*C*) of DMN. (*A*) Normalized fura-2 fluorescence signals excited by continuous illumination at 380 nm. Seven recordings from five cells are superimposed. The 380-nm light was turned on at zero time. The pipette solution was solution B (Table 1). (*B*) Calculated $[Ca^{2+}]_i$ wave from the average of *A* (·····). The rate of $[Ca^{2+}]_i$ change ($d[Ca^{2+}]_i/dt$) was estimated from the line fit (– – –) over 0.1–0.3 s. The solid lines are computer simulations under the same recording solution by assuming different on rates for DMN. The measured $[Ca^{2+}]_i$ is best fitted with an on rate of 3.2 × 10^7 M^{-1} s^{-1}. (*C*) Relaxation rates (○) versus $[Ca^{2+}]_i$ for fitting the on rate of DMN. The processing of data was the same as in Fig. 1 *B*. The solid line is the fit according to Eq. 9. The pipette solution was solution C (Table 1).

low-pass filtering response of the PMT, which are not represented in the simulations, cause some delay in the measured trace.

We further studied the on rate of DMN by applying Eq. 9 using flash photolysis. The pipette solution was solution C of Table 1. With this solution, the basal $[Ca^{2+}]_i$ is clamped to 49 nM. According to Eq. 15, 4 mM DMN will give rise to a Ca^{2+} binding ratio of 6800. A similar binding ratio is calculated for 2 mM fura-2. Thus both species compete for binding of calcium. Howerver, because of a very high Ca^{2+} binding rate, Ca^{2+} is taken up by fura-2 immediately after the flash and, later on, partitioned to unphotolyzed DMN. This slow back relaxation has a time constant in the range of hundreds of milliseconds. Therefore, a 5% ND filter had to be inserted in the fura-2 excitation pathway to reduce the photolysis by the fura-2 measuring light to an extent where it was negligible. The measured fura-2 relaxation rates at different $[Ca^{2+}]_i$ from nine cells are plotted versus $[Ca^{2+}]_i$ in Fig. 2 *C*. By fitting the data according to Eq. 9, we obtained a value of 3.5 × 10^7 M^{-1} s^{-1} for α_N, which is quite close to our result above.

The apparent K_d and concentration of the endogenous Ca^{2+} buffer

If the endogenous Ca^{2+} buffer is the predominant Ca^{2+} buffer and DMN is fully loaded with Ca^{2+}, we can release Ca^{2+} slowly by photolyzing DMN using steady-state UV illumination and "titrate" the endogenous Ca^{2+} buffer to study its apparent dissociation constant ($K_{d,E}$) and its total concentration ($[E]_T$). Solution D in Table 1 is used for this purpose for the following reasons: 1) a high concentration of DMN almost fully loaded ensures that a large amount of Ca^{2+} can be released and minimizes the buffering capacity of DMN; 2) the basal $[Ca^{2+}]_i$ is clamped around 100 nM; 3) a relatively low concentration of furaptra is used to minimize its buffering capacity. However, the indicator concentration cannot be set too low, because of the influence of DMN and its photoproducts on the $[Ca^{2+}]_i$ measurement (Zucker, 1992). These conditions are optimal for "titrating" the endogenous buffer by releasing Ca^{2+} from DMN and using furaptra as an indicator. For this purpose, a steady UV light (380 nm) was turned on at time 0 in Fig. 3 *A*, causing the fluorescence of furaptra to drop as Ca^{2+} was released from DMN. Because the rate of equilibration of Ca^{2+} with the endogenous Ca^{2+} buffer and furaptra is much faster than the release rate of Ca^{2+} (1.5 s^{-1}), we can use the equilibrium equation (Eq. 24) to describe this process. By setting $[Ca]_{T,t}$ to 4.8 mM, including buffers N, E, Fp, P in Eq. 24, and assuming $K_{d,Fp}$ = 50 μM, $K_{d,N}$ = 5 nM, $K_{d,P}$ = 3 mM (Kaplan and Ellis-Davies, 1988), we fit the fluorescence signals of furaptra using $K_{d,E}$ and $[E]_T$ as free parameters. A sample fit is presented in Fig. 3 *B*, resulting in a $K_{d,E}$ of 134 μM and an $[E]_T$ of 4.75 mM. The average values from 12 cells were 129 ± 35 μM for $K_{d,E}$ and 5.1 ± 1 mM for $[E]_T$ (mean ± SD). Interestingly, if we divide $[E]_T$ by $K_{d,E}$, which will give an estimate of the binding ratio of the endogenous Ca^{2+} buffer, we obtain 39.5, a value quite close to that of Zhou and Neher (1993). In six other cells that were perfused with 2 μM CCCP, we found nearly the same numbers, 125.9 ± 24.6 for $K_{d,E}$ and 4.38 ± 0.8 mM for $[E]_T$ (mean ± SD), which suggested that our estimate was not contaminated by mitochondrial Ca^{2+} uptake (see below).

This low affinity and high concentration of the endogenous Ca^{2+} buffer were further confirmed by the following flash experiments. The flash lamp was fixed at 300-V discharge, and the photolysis efficiency was changed by inserting different ND filters of 10%, 20%, 25%, 50%, and 100% transmission. By measuring the $[Ca^{2+}]_i$ immediately

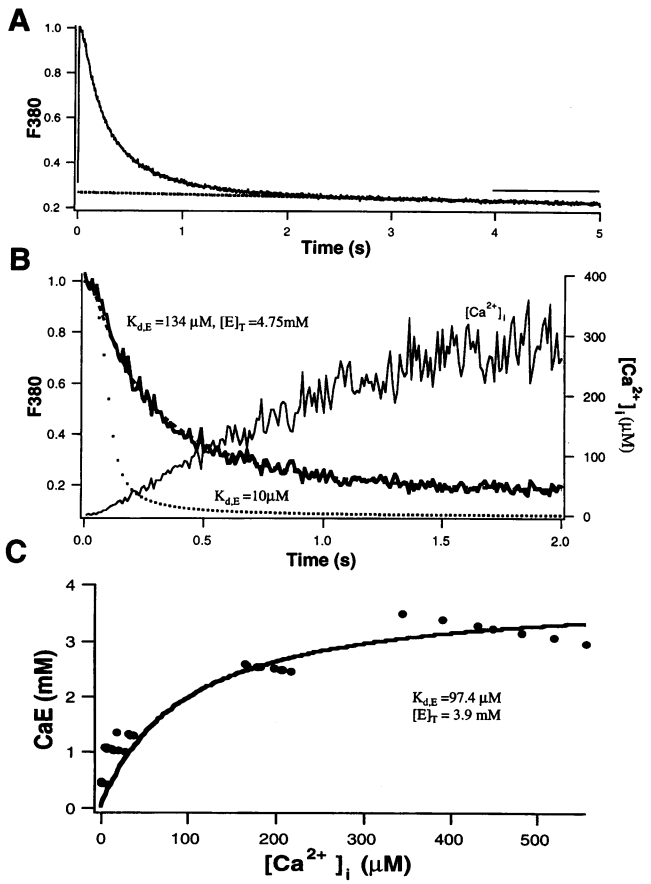

FIGURE 3 The properties of the endogenous Ca^{2+} buffer. (*A*) Normalized furaptra fluorescence signals excited at 380 nm in the presence of 96% loaded 5 mM DMN. The pipette solution was solution D (Table 1). The 380-nm light was turned on at zero time, and the fluorescence decreased because of the photorelease of Ca^{2+} from DMN. A line fit to the function $F_{380}(t) = c(1 - rt)$ was performed in the time window of 4–5 s (indicated by *bar* in the figure) when DMN was totally photolyzed and the small change in fluorescence reflected the bleaching and other nonspecific changes. The rate of this small change r was determined from the line fit, and the original fluorescence trace F_{380} was corrected as follows: $F'_{380} = F_{380}(1 + rt)$. F'_{380} was then used during analysis. Because the basal $[Ca^{2+}]_i$ was ~100 nM, which means $F(0)$ approaches F_{max} for furaptra fluorescence excited at 380 nm, Eq. 6 was applied to calculate the $[Ca^{2+}]_i$ in the entire time window after correction for bleaching and nonspecific fluorescence. The fluorescence of DMN and its photoproducts were estimated in control experiments using the same internal solution, excluding furaptra. DMN (5 mM) was found not to be fluorescent at all as compared with 0.2 mM furaptra. The fluorescence of photoproducts of 5 mM DMN was only 1.8% (n = 3) of the fluorescence of 0.2 mM furaptra. It should be pointed out that the fluorescent traces for this study were recorded after 10 min of whole-cell recording, when the fast mitochondrial uptake should have vanished in the absence of ATP (see Results). (*B*) The same fluorescence trace (*thick solid line*), after correction, as described in *A* on an expanded time scale. The trace is fitted very well (*superimposed dashed line*) by assuming an endogenous Ca^{2+} buffer with a total concentration of 4.75 mM and a K_d of 134 μM. A fit assuming a K_d of 10 μM and a total concentration of 0.4 mM is also shown (*dashed line below the fluorescence trace*). The thin line is the $[Ca^{2+}]_i$ calculated from the fluorescence signal. (*C*) Analysis of the properties of endogenous buffer using flash experiments. The concentrations of Ca^{2+} bound form of buffer (●) are plotted versus $[Ca^{2+}]_i$ measured according to Eq. 3. The solid line is a fit made assuming a binding ratio of 40.

after the flash, we could calculate how much Ca^{2+} bound to furaptra, DMN, and photoproducts of DMN. The amount of Ca^{2+} bound to the endogenous Ca^{2+} buffer ([CaE]) is then determined by Eq. 24 and is plotted versus $[Ca^{2+}]_i$. Data from nine cells are presented in Fig. 3 *C*. Setting the binding ratio of the endogenous Ca^{2+} buffer to 40, we fit the data in Fig. 3 *C* according to

$$[CaE] = \frac{[Ca^{2+}]_i \cdot [E]_T}{[Ca^{2+}]_i + K_{d,E}} \tag{26}$$

and obtain 97.4 μM for $K_{d,E}$ and 3.9 mM for $[E]_T$, which is consistent with our study using steady UV photolysis.

Ca^{2+} binding kinetics of the endogenous Ca^{2+} buffer

Let X in Eq. 9 be the endogenous Ca^{2+} buffer (E). Close examination of Eq. 9 shows that, at higher $[Ca^{2+}]_i$ levels, the fura-2 relaxation rate will be a linear function of $[Ca^{2+}]_i$. However, the linearity will not hold any more in the lower $[Ca^{2+}]_i$ range. The fura-2 relaxation rate will not decrease with lowering $[Ca^{2+}]_i$ in the lower $[Ca^{2+}]_i$ range; instead, it will bend upward because of the influence of the endogenous Ca^{2+} buffer. Therefore, we studied the relaxation of fura-2 while photoreleasing Ca^{2+} to achieve $[Ca^{2+}]_i$ in the range of several hundreds of nM. The on rate of the endogenous Ca^{2+} buffer, then, can be estimated according to Eq. 9.

Accordingly, we included 1 mM DMN, 1 mM $CaCl_2$, and 0.1 mM fura-2 in the pipette for studying the Ca^{2+} binding kinetics of the endogenous Ca^{2+} buffer. The reason for using 0.1 mM fura-2 instead of 50 μM is to enlarge λ_F. However, the dye concentration should not be increased too much, so that the fluorescence relaxation will not be too fast to be measured. In Fig. 4 *A*, the relaxation rates of fura-2 are plotted against $[Ca^{2+}]_i$. The data were collected from 12 cells; each point was calculated as the average of at least five traces. By assuming 100 μM for $K_{d,E}$ and 4 mM for $[E]_T$, the data are best fitted with an α_E of 1.07×10^8 M^{-1} s^{-1}. This fast on rate is further supported by extrapolating the fitted curve to the time where flash light intensity reaches its mean value, as shown in Fig. 4 *B*. For a steplike increase in $[Ca^{2+}]_i$, this extrapolation is expected to agree with the initial fluorescence value before the flash. If, however, there is a $[Ca^{2+}]_i$ spike during the flash, which according to computer kinetics simulation is the case for $\alpha_E < 1 \times 10^8$ M^{-1} s^{-1}, this extrapolation will fall below its preflash value because of accelerated Ca^{2+} binding to fura-2 during the $[Ca^{2+}]_i$ spike. But we never saw such an extrapolation in our data, which in turn suggests that $\alpha_E \geq 1 \times 10^8$ M^{-1} s^{-1}.

Kinetic study of Ca^{2+} uptake by mitochondria

While using the steady UV photolysis protocol in the absence of ATP, we sometimes observed at the beginning of

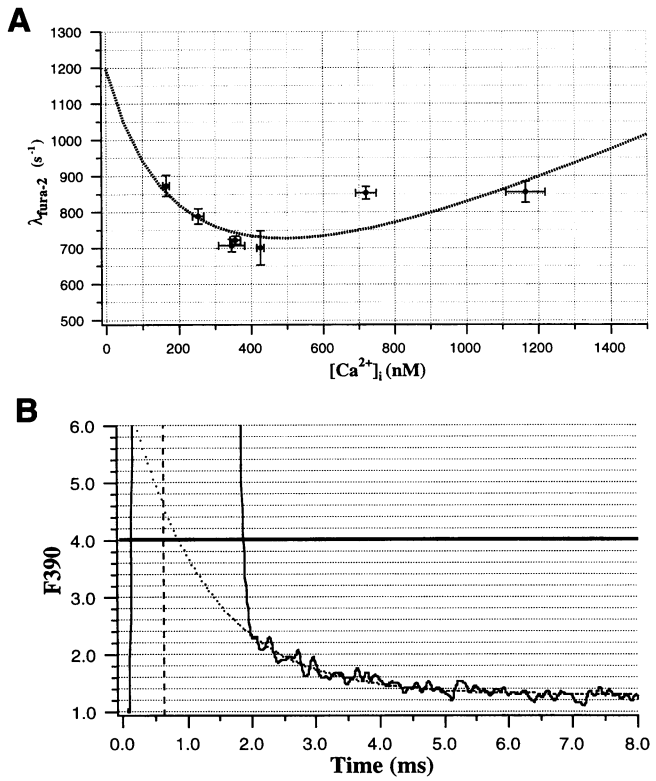

FIGURE 4 Analysis of Ca^{2+} binding kinetics of endogenous buffer. (*A*) The recording condition and the processing of data were the same as in Fig. 1, except that we used a higher concentration of fura-2 (0.1 mM) and examined the relaxations at lower $[Ca^{2+}]_i$ levels, to see the influence of the endogenous Ca^{2+} buffer on the relaxation rate. The data were best fitted by an on rate of 1.07×10^8 M^{-1} s^{-1} for the endogenous buffer (·····). The concentrations of Ca^{2+} buffer and its K_d were set to 4 mM and 100 μM, respectively. (*B*) Fluorescence relaxation signal (——) elicited by a flash triggered at zero time. Superimposed (·····) is a single exponential fit to the 2–8-ms time window after the decay of the flash light artifact and its extrapolation to zero time. The $[Ca^{2+}]_i$ corresponding to the steady-state level of this trace was 1164 nM, and the relaxation rate was 855.1 s^{-1}. The fluorescence signal is given in arbitrary units. The horizontal thick line indicates the fluorescence intensity just before the flash. The vertical dashed line indicates the time when the integrated flash light reached its half-maximum value.

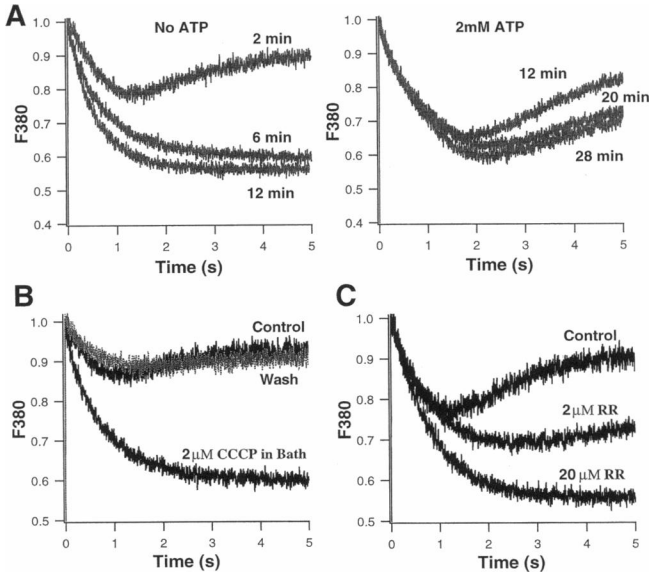

FIGURE 5 Identification of mitochondrial Ca^{2+} uptake. (*A*) Fluorescence signals excited at 380 nm in the presence of 1 mM fully loaded DMN. Each panel shows recordings from one cell at different times after forming whole cell in the absence (*left*) and presence (*right*) of ATP in the pipette. The initial decrease in fluorescence corresponds to the photorelease of Ca^{2+} from DMN. The latter rebound reflects the Ca^{2+} uptake after DMN was totally photolyzed. (*B*) The block of Ca^{2+} uptake by local perfusion of 2 μM CCCP. A pipette of 10-μm tip diameter was used to apply CCCP. Several minutes after a control recording, CCCP was puffed toward the cell. After the $[Ca^{2+}]_i$ transient, caused by the puff of CCCP, had declined, a second measurement was carried out. Then the pipette for applying CCCP was removed to observe the recovery of mitochondrial uptake. (*C*) The block of Ca^{2+} uptake by ruthenium red. Ruthenium red at different concentrations (as indicated in the figure) was included in the internal solution. The results were from three cells recorded at the same time after forming whole cell.

whole-cell recordings that furaptra fluorescence, excited at 380 nm, did not remain at a low value after all of the DMN was photolyzed. Rather, it bent up again, reflecting a $[Ca^{2+}]_i$ drop. This suggests that some fast Ca^{2+} clearance mechanism exists in our cells. We then found that this clearance mechanism vanished within several minutes of whole-cell recording when ATP was not present in the internal solution. In contrast, it could be maintained even for half an hour in the presence of either 1 mM MgATP plus 1 mM Na_2ATP or 2 mM Na_2ATP, as shown in Fig. 5 *A*. This clearance of Ca^{2+} could be blocked by local perfusion with 2 μM CCCP ($n = 3$; a recording from one cell is shown in Fig. 5 *B*). It could be largely reduced by including 2 μM ruthenium red (RR) in the pipette ($n = 5$) and totally blocked by 20 μM RR ($n = 3$), as shown in Fig. 5 *C*. The results suggest that this fast clearance of Ca^{2+} is due to mitochondrial Ca^{2+} uptake (Missiaen et al., 1993; Park et al., 1996). This is in accordance with recent findings in rat chromaffin cells (Herrington et al., 1996; Park et al., 1996).

It is interesting to know the extent to which this mitochondrial Ca^{2+} uptake will affect the $[Ca^{2+}]_i$ after a flash. In Fig. 6 *A*, we used an internal solution containing 1 mM DMN, fully loaded with Ca^{2+}, 500 μM furaptra, and 2 mM ATP, to study the $[Ca^{2+}]_i$ decay after a flash. A 10% ND filter was inserted into the fluorescence excitation pathway, thus allowing fast $[Ca^{2+}]_i$ measurement by the single-wavelength method. In five cells studied, the $[Ca^{2+}]_i$ showed fast decays, with an average half-time of 1.07 ± 0.56 s for an initial $[Ca^{2+}]_i$ of 16 ± 3.2 μM (mean ± SD) after 100% photolysis of DMN. This fast decay could be changed to a slow one with a time constant of tens of seconds by local perfusion of 2 μM CCCP, as shown in Fig. 6 *B* ($n = 3$).

For measuring the V_{max} of this mitochondrial Ca^{2+} uptake, we included solution E (Table 1) in the pipette to reach high levels of $[Ca^{2+}]_i$ by flash photolysis and to fulfill the condition of $[Ca^{2+}]_i^2 \gg K_{1/2}^2$ (Eq. 18). In Fig. 7 *A* we can observe a linear decay in $[Ca^{2+}]_i$, as predicted by Eq. 21. V_{max} is then measured according to Eq. 21 by a linear fit to

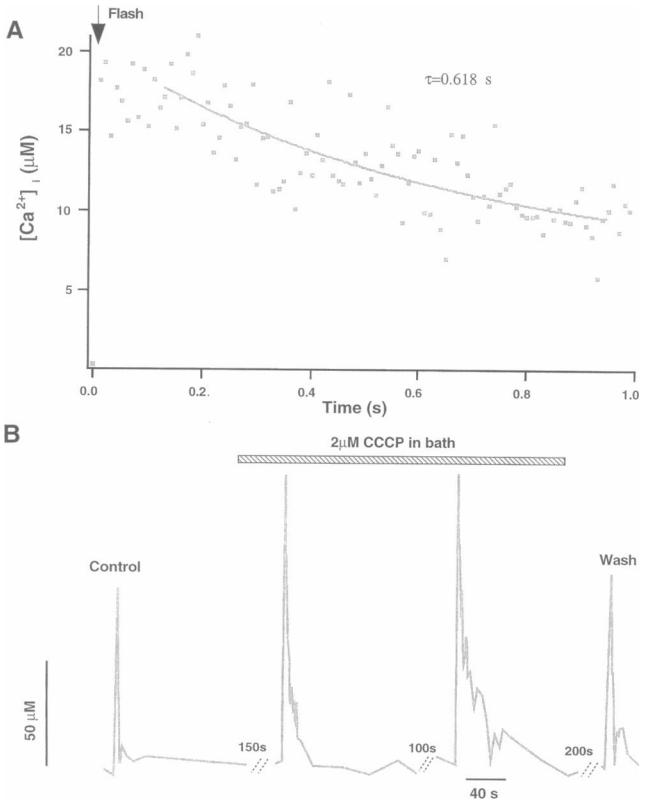

FIGURE 6 Influence of mitochondrial Ca^{2+} uptake on the $[Ca^{2+}]_i$ time course after a flash. (*A*) Fast $[Ca^{2+}]_i$ decay (*squares*) after a flash triggered at zero time. Superimposed is a single exponential fit (*curve*) with a time constant of 0.618 s. (*B*) Prolongation of the $[Ca^{2+}]_i$ decay after flashes by CCCP. Four repetitive $[Ca^{2+}]_i$ traces recorded in one cell are shown. Flashes were given as indicated by the arrows. The fast $[Ca^{2+}]_i$ decay could be retarded several seconds by local perfusion of 2 μM CCCP in the bath as indicated in the figure.

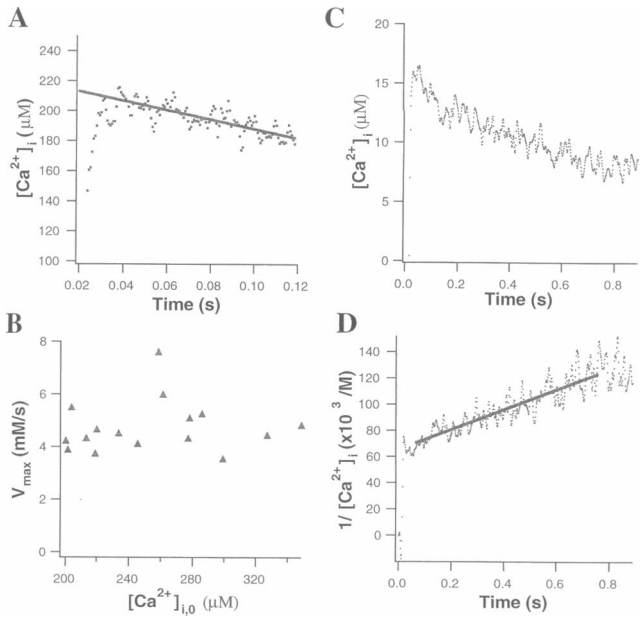

FIGURE 7 Kinetic analysis of mitochondrial Ca^{2+} uptake. The pipette solution was solution E (Table 1). (*A*) $[Ca^{2+}]_i$ decay at high $[Ca^{2+}]_i$ level after a flash triggered at 20 ms. The rate of $[Ca^{2+}]_i$ decay is estimated by a line fit (*superimposed solid line*) from 40 ms to 120 ms. (*B*) Measured V_{max} values from 13 cells were plotted against their initial $[Ca^{2+}]_{i,0}$. $[Ca^{2+}]_{i,0}$ was calculated by extrapolating the line fit as shown in *A* to 20 ms. For calculating the binding ratio of a given Ca^{2+} chelator, say X, the following formula was used:

$$\kappa_X = \frac{[X]_T/K_{d,X}}{(1 + [Ca^{2+}]_a/K_{d,X}) \cdot (1 + [Ca^{2+}]_b/K_{d,X})}$$

where $[Ca^{2+}]_a$ and $[Ca^{2+}]_b$ are free $[Ca^{2+}]$ values at the start and the end of the line fit as shown in *A*. (*C*) $[Ca^{2+}]_i$ decay at relatively low $[Ca^{2+}]_i$ levels after a flash triggered at 20 ms. (*D*) The reciprocal of the $[Ca^{2+}]_i$ trace in *C*. Superimposed is the line fit according to Eq. 22.

the $[Ca^{2+}]_i$ decay within a time window of 100 ms after the flash. To test whether, at this $[Ca^{2+}]_i$ level, the mitochondrial $[Ca^{2+}]_i$ uptake rate is really V_{max}, the measured V_{max} values from 13 cells are plotted against their initial $[Ca^{2+}]_{i,0}$ level immediately after flashes (Fig. 7 *B*). A constant V_{max} can be observed when $[Ca^{2+}]_{i,0}$ was varied between 200 and 350 μM. This indicates that the Ca^{2+} uptake rate is saturated in this $[Ca^{2+}]_i$ range. The average value of V_{max} from the data in Fig. 7 *B* is 4.76 ± 1 mM/s (mean ± SD, n = 16).

In the preliminary measurements using continuous UV photolysis as shown in Fig. 5, we fitted the total Ca^{2+} uptake by mitochondria as a function of $[Ca^{2+}]_i$ according to Eqs. 23 and 24 and obtained an estimate of ~50 μM for $K_{1/2}$. We then used the same internal solution as that used in Fig. 6 *A* to study the $[Ca^{2+}]_i$ decay after flashes at low $[Ca^{2+}]_i$ levels. One example is shown in Fig. 7 *C*. The reciprocal of the $[Ca^{2+}]_i$ in Fig. 7 *C* is plotted in Fig. 7 *D*, where a linear increment as a function of time is observed, as one would expect from Eq. 22. The measured rate of the increment in the reciprocal of $[Ca^{2+}]_i$ in this type of study is, on average, 70,597 ± 26,794 $M^{-1}\,s^{-1}$ (mean ± SD, n = 9). $K_{1/2}$ is then calculated to be 36.7 μM, according to Eq. 22.

When we looked at the $[Ca^{2+}]_i$ decay during a relatively long time span (500 ms) under the same conditions as in Fig. 7 *A*, we saw a linear $[Ca^{2+}]_i$ decline within the first 100 ms. Later, as shown in Fig. 8 *A*, the rate of decay was retarded to some extent, even when $[Ca^{2+}]_i$ was still high enough for Eq. 21 to hold. This suggests saturation of mitochondrial uptake. We then calculated the total amount of Ca^{2+} taken up by mitochondria according to Eq. 23 and compared it with theoretical predictions using our measured values of V_{max} and $K_{1/2}$, as shown in Fig. 8 *B*. It is seen that the measured total Ca^{2+} uptake by mitochondria (*dashed line*) begins to deviate from the theoretical solid line when mitochondria sequester as much as 0.5 mM total intracellular Ca^{2+}. At 1 mM total intracellular Ca^{2+}, uptake almost ceases, suggesting that mitochondria have a capacity of taking up ~1 mM total Ca^{2+}. Similar capacities were observed in six cells.

DISCUSSION

Quantitative understanding of cellular Ca^{2+} signals, which are shaped both by Ca^{2+} fluxes across various types of

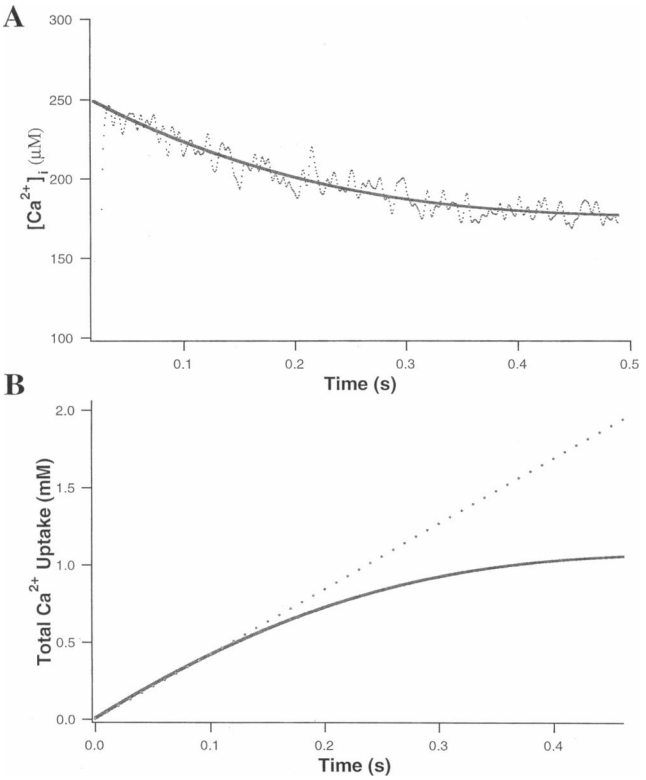

FIGURE 8 Capacity of mitochondrial Ca^{2+} uptake. The pipette solution was solution E (Table 1). (*A*) $[Ca^{2+}]_i$ time course after flash. The trace is smoothed by fitting a fourth-order polynomial (*superimposed solid line*). (*B*) The dashed line is the calculation of total Ca^{2+} uptaked by mitochondria using the smoothed trace in *A*. The theoretical prediction of mitochondrial Ca^{2+} accumulation according to our kinetic parameters of mitochondrial uptake is also plotted (*solid line*).

membranes and by Ca^{2+} binding to cytosolic Ca^{2+} buffers, requires detailed knowledge of both kinetic and steady-state properties of the individual mechanisms involved. Here we show that, in individual bovine chromaffin cells, under the whole-cell patch-clamp condition, many of the relevant parameters can be determined quantitatively by a combination of fluorometric Ca^{2+} measurement, using either fura-2 or furaptra, and photolysis of the caged-Ca^{2+} compound DM-nitrophen, using either flash or continuous (steplike onset) illumination. Pipette filling solutions containing combinations of indicator dye and caged compound can be formulated that allow the "titration" of the endogenous buffer and the interpretation of relaxations of the indicator dye fluorescence in terms of kinetic rate constants. Essential for these procedures are 1) a careful in vivo calibration of the indicator dyes, which in turn can be used to calibrate both the flash lamp and the continuous light source; 2) a continuous light source that photolyzes the caged compound in a time much shorter than the diffusional exchange time between pipette and cytosol; 3) the fact that DM-nitrophen, in the absence of Mg^{2+}, has a very high Ca^{2+} affinity, such that at several hundred nM basal $[Ca^{2+}]_i$ it is present almost exclusively in the Ca^{2+}-bound form. The latter feature restricts some of the measurements that we performed to conditions without Mg^{2+}. However, it allows DM-nitrophen to be used as a light-dependent Ca^{2+} source, which itself contributes only very little to Ca^{2+} buffering. An important aspect providing simplicity of the analysis and formal description of our results is the finding that, in bovine chromaffin cells, the sum of all endogenous Ca^{2+} buffers (under the conditions of our experiments) can be described by a single low-affinity species with a dissociation constant of ~100 μM. Thus most of the equations for buffering and fluxes are linear below 100 μM $[Ca^{2+}]_i$, and binding/unbinding reactions to the endogenous buffers are fast.

Once Ca^{2+} buffers have been characterized, Ca^{2+} fluxes can be measured quantitatively and conditions can be identified, which make it possible to impose steplike changes on the $[Ca^{2+}]_i$ time course for the analysis of Ca^{2+}-dependent cellular responses. Of particular concern is the possibility of spikelike overshoots during flashes and limited duration of $[Ca^{2+}]_i$ elevations after flashes, as described below.

Are large Ca^{2+} spikes associated with photolyzing flashes?

Zucker (1993) and Escobar et al. (1995) showed in in vitro experiments that UV flashes of DM-nitrophen containing solutions could generate large (tens or hundreds of μM) $[Ca^{2+}]_i$ spikes of milliseconds duration at the onset of steplike $[Ca^{2+}]_i$ increases. This was attributed to the relatively slow Ca^{2+} rebinding to unphotolyzed DM-nitrophen compared with the fast photolytic release of Ca^{2+}. In other in vivo experiments, 10 mM fully loaded DM-nitrophen and millimolar amounts of the calcium chelator DPTA were used (Heinemann et al., 1994) to generate larger steplike $[Ca^{2+}]_i$ increases for kinetic studies of secretion in bovine chromaffin cells. With this fully Ca^{2+} loaded DM-nitrophen, the existence of significant $[Ca^{2+}]_i$ spikes depends on whether binding of Ca^{2+} to the endogenous Ca^{2+} buffer and to DPTA is slower or faster than the rate of photorelease of Ca^{2+}. Assuming 0.4 mM endogenous fixed Ca^{2+} buffer with a K_d of 10 μM and an on rate of 10^7 M^{-1} s^{-1}, an on rate of 1.5×10^6 M^{-1} s^{-1} for DMN, and an on rate of 10^7 M^{-1} s^{-1} for DPTA, Heinemann et al. (1994) performed simulations of the Ca^{2+} time course for solutions containing 10 mM Ca^{2+}-saturated DM-nitrophen and 10 mM DPTA. The simulations showed that there should be a Ca^{2+} spike to 80 μM lasting ~1–2 ms if a flash were applied to raise $[Ca^{2+}]_i$ to a step level of 15 μM. Such a Ca^{2+} spike would significantly shorten the delay of membrane capacitance (C_m) responses according to the same authors' kinetic model of exocytosis. But experimentally, such a shortening of the delay was not found. A similar discrepancy was found for the simulated Ca^{2+} time courses and the C_m responses of Neher and Zucker (1993). It was suggested that the submembrane Ca^{2+} spike was not as large as expected, because of the existence of a localized submembrane Ca^{2+} buffer of sufficiently high concentration and fast on rate.

In this study we used DM-nitrophen to homogeneously increase $[Ca^{2+}]_i$ and found that the endogenous Ca^{2+} buffer in bovine chromaffin cells is of high concentration and fast kinetics. To understand the extent to which the presence of this fast endogenous buffer will help to address the above discrepancy, we performed simulations for the pipette solution of Heinemann et al. (1994), using our new estimates of the kinetic parameters. These are 4 mM endogenous fixed Ca^{2+} buffer with a K_d of 100 μM and 10^8 M^{-1} s^{-1} on rate, a 4×10^7 M^{-1} s^{-1} on rate for DMN, and a 10^7 M^{-1} s^{-1} on rate for DPTA. The results of these simulations are shown in Fig. 9. The dotted line is the time course of a flash from our Rapp flash lamp, as measured with a fast photodiode. The flash is triggered at 2 ms. With an increase in $[Ca^{2+}]_i$ to a step level of 14 μM, there is an overshoot of only 8 μM (peak) for 750 μs (half-width). Such a spike will not significantly accelerate the early rise (first 10 ms) of the C_m responses simulated by using the secretory kinetic model of Heinemann et al. (1994). Even with a steplike change in $[Ca^{2+}]_i$ to 40 μM, there is an overshoot in $[Ca^{2+}]_i$ of no more than 20 μM. A similar simulation was done for 8.5 mM DM-nitrophen loaded with 3 mM Ca^{2+}, with a 50% photolysis efficiency, which resembles the condition used by Neher and Zucker (1993). The result is shown as a dashed line in Fig. 9. The Ca^{2+} spike is only 10 μM for less than 1 ms (half-width), which would produce only a sub-fF secretion, according to the model of Heinemann et al. (1994). It will further be reduced if the on rate of DPTA is higher ($\geq 4 \times 10^7$ M^{-1} s^{-1}), as suggested by recent T-jump studies (M. Naraghi, personal communication). Thus the former disagreement between the experimental data and the simulations can be accounted for by our evidence for the existence of a fast and high concentration of an endogenous Ca^{2+} buffer in bovine chromaffin cells.

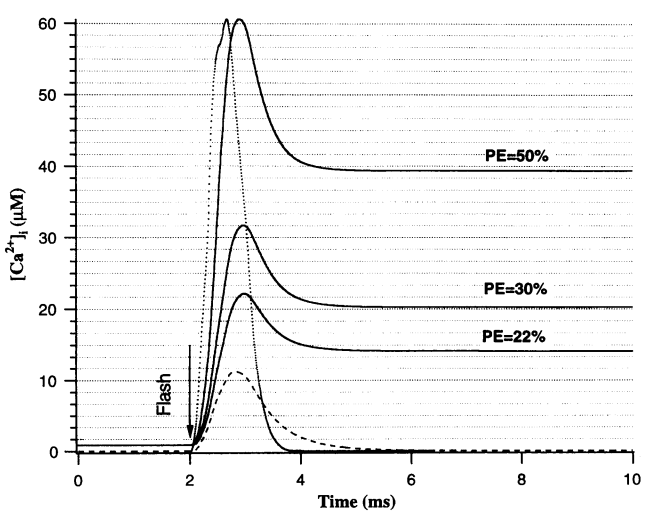

FIGURE 9 Simulations of Ca^{2+} spikes during flash experiments. The dotted line is the time course of the flash lamp. The solid lines are simulations of in vivo $[Ca^{2+}]_i$ time courses generated by flashes at different photolysis efficiencies (PE in figure). The pipette solution for solid lines contained 10 mM fully loaded DMN, 1 mM furaptra, and 10 mM DPTA, which was the condition used by Heinemann et al. (1994). Kinetic parameters were chosen as indicated in the text. The dashed line is the simulation of a pipette solution containing 8.5 mM DMN, 3 mM total Ca^{2+}, and 0.3 mM furaptra with 50% photolysis efficiency, which was the condition used by Neher and Zucker (1993).

Time course of $[Ca^{2+}]_i$ decay after flash photolysis of caged Ca^{2+}

Different studies report widely varying rates of $[Ca^{2+}]_i$ decline after rapid elevation by flash photolysis using different compositions of internal solutions. This decay in $[Ca^{2+}]_i$ can potentially alter the kinetics of the exocytotic burst and distort the estimate of slow exponential components. For internal solutions without ATP, the time constant of $[Ca^{2+}]_i$ decline was 20.1 s on average in bovine chromaffin cells, according to Heinemann et al. (1994). However, in a recent paper by Gillis et al. (1996), faster $[Ca^{2+}]_i$ declined to levels too low to be measured by furaptra. These studies were performed in MgATP-containing solutions, and time constants of about 1 s were measured. One possible source of this rapid decay in $[Ca^{2+}]_i$ might be the complex chelating reaction that takes place in MgATP-containing solutions. Because DMN can also bind Mg^{2+}, upon flash photolysis of DMN, a fraction of the released Ca^{2+} can displace Mg^{2+} bound to DMN. However, because the kinetics of Mg^{2+} binding to DMN and ATP are unknown, it is hard to predict how long this exchange will take. But this explanation does not seem to be valid in this case, because our calculations suggest that the drop in $[Ca^{2+}]_i$ would not be nearly as large as what was measured (see also Gillis et al., 1996). In our study, using 2 mM Na_2ATP without Mg^{2+}, we also observed a fast $[Ca^{2+}]_i$ decay within seconds, which we showed to be mainly due to the mitochondrial uptake in the presence of ATP, because local perfusion of 2 μM CCCP prolonged the $[Ca^{2+}]_i$ decay to many tens of seconds. Our estimate of the kinetics of mitochondrial Ca^{2+} uptake also suggests that it may play a significant role in the clearance of Ca^{2+} when $[Ca^{2+}]_i$ is in the tens of μM range under conditions in which the function of mitochondria is maintained. Thus, when using ATP-containing internal solution for clamping $[Ca^{2+}]_i$ to high levels by caged Ca^{2+}, care should be taken to allow for the fast Ca^{2+} uptake by mitochondria. For instance, if one aims at elevating $[Ca^{2+}]_i$ to the 10 μM range and maintaining it for several seconds, the $[Ca^{2+}]_i$ dynamics can be approximated by Eq. 22. According to Eq. 22, one way to slow down the $[Ca^{2+}]_i$ decay is to enlarge the binding ratio of added exogenous Ca^{2+} buffer. This in turn requires that large amounts of DMN have to be used to reach the desired $[Ca^{2+}]_i$ level. Then the release of more Ca^{2+} into the cytosol will cause the depletion of the capacity of mitochondrial Ca^{2+} uptake and result in a decline rate even smaller than that predicted by Eq. 22.

Properties of the endogenous Ca^{2+} buffer

The thought that cytoplasmic Ca^{2+} buffers play an important role in shaping $[Ca^{2+}]_i$ signals led to a number of quantitative Ca^{2+} binding ratio measurements in neurons (Müller et al., 1993; Fierro and Llano, 1996; Tatsumi and Katayama, 1993) and adrenal chromaffin cells. In previous work of Neher and Augustine (1992) and Zhou and Neher (1993), an immobile buffer with a Ca^{2+} binding ratio of 40 was found in bovine chromaffin cells. This was assumed to have low affinity, because no decrease in the binding ratio was found, even when basal $[Ca^{2+}]_i$ reached levels as high as 3 μM. Here we used two methods to estimate more accurately the affinity of this buffer at higher $[Ca^{2+}]_i$ concentrations. In one method, steady UV light was applied to photorelease Ca^{2+} on a relatively slow time scale. The single-wavelength method was used to monitor $[Ca^{2+}]_i$ in a time window of 3 s. This, actually, was like a titration of the endogenous Ca^{2+} buffer. Because this method required a relatively long time span, the results might have been contaminated by fast Ca^{2+} clearance mechanisms. We generally used this method 10 min after obtaining the whole-cell configuration and did not include ATP in the pipette solution. Under these conditions, we have shown the fast Ca^{2+} uptake by mitochondria not to be of significant magnitude. Furthermore, some measurements were made in the presence of CCCP in the bath and no difference was found. Other Ca^{2+} clearance mechanisms like Na^+-Ca^{2+} exchange, plasma membrane Ca^{2+}-ATPase, and ER/SR Ca^{2+}-ATPase seem unlikely to make major contributions because of their low clearance rates (Missiaen et al., 1993; Park et al., 1996), especially in the absence of ATP.

Our second method applied flash photolysis for fast elevation of $[Ca^{2+}]_i$ within milliseconds. Because $[Ca^{2+}]_i$ was measured immediately after flashes, the Ca^{2+} clearance mechanisms should be negligible. This method, however, relies on the accurate determination of flash photolysis efficiency. Although both methods have their own limitations, the good correspondence between the two estimates supports the approach taken. It should be pointed out that for both methods, we had to assume that the K_d of the furaptra and of photoproducts of DMN was the same in the cytoplasm as in vitro, which might not be the case. But because the endogenous buffer was the dominant buffer in our measuring situation compared with furaptra (binding ratio of 4) and photoproducts of DMN (binding ratio of 3 after 100% photolysis), the influence of the latter chelators may not be significant. Actually, when we changed the K_d of furaptra from 50 μM to 100 μM in Eq. 24, the estimate for the K_d of endogenous buffer was not altered significantly.

Unlike in the case of molluscan neurons (Ahmed and Connor, 1988), ventricular myocytes (Berlin et al., 1994) and *Myxicola infudibulum* giant axons (Al-Baldawi and Abercrombie, 1995), where buffering capacities were found to decrease when $[Ca^{2+}]_i$ rose, our endogenous buffer in bovine chromaffin cells has a low affinity of 100 μM, which is compatible with Zhou and Neher (1993) and the "X" buffer of squid axon postulated by Brinley et al. (1977). The measured properties of the buffers may provide some clues to their chemical nature. In addition to synexin and troponin-c-like proteins proposed by Neher and Augustine (1992), some membrane- and cytoskeleton-related calmodulin or calmodulin-like proteins may also be candidates. Calmodulin is an EF-hand protein found in all eukaryotic organisms, in both cytoslic and membrane-associated form. It contains two low-affinity (K_d 10–100 μM) sites at its N-terminal (Weinstein and Mehler, 1994) and has an on rate of $5 \times 10^8\ M^{-1}\ s^{-1}$ (Falke et al., 1994). Some calmodulin-like proteins also have a low affinity for Ca^{2+} (K_d 250 μM; Durussel et al., 1993), which is compatible with our finding.

The existence of such a low-affinity Ca^{2+} buffer with 4 mM binding sites also has an impact on the calibration of the $[Ca^{2+}]_i$ measurement using furaptra in flash experiments. Ten millimolar DPTA is not sufficient to overcome this endogenous Ca^{2+} buffer. It is safe to use 40 mM DPTA or more, which gives a binding ratio 10-fold higher than that of the endogenous Ca^{2+} buffer for the calibration of K_{eff} after flash.

Comparison of kinetic studies in vivo with those in vitro

Because the properties of Ca^{2+} chelators may change in vivo by binding to unknown intracellular structures (Baylor and Hollingworth, 1988; Hove-Madsen and Bers, 1992), it is interesting to compare our in vivo kinetic data with data derived in vitro. Our in vivo dissociation constant of fura-2 is consistent with that of Zhou and Neher (1993) and not very different from in vitro values. Our measured on rate of fura-2 is similar to the in vitro data ($5 \times 10^8\ M^{-1}\ s^{-1}$) by Jackson et al. (1987) and slightly lower than $6 \times 10^8\ M^{-1}\ s^{-1}$, given by Kao and Tsien (1988) from in vitro T-jump experiments. Thus fura-2 seems to be less influenced by intracellular constituents in adrenal chromaffin cells than in muscle cells (Baylor and Hollingworth, 1988; Blatter and Wier, 1990).

Zucker (1993), using an in vitro steady UV photolysis method, measured the on rate of DMN and obtained a value of $1.5 \times 10^6\ M^{-1}\ s^{-1}$. This is like EGTA, but smaller than the values obtained in two other studies (Escobar et al., 1995; Ellis-Davies et al., 1996), in which an on rate of $8 \times 10^7\ M^{-1}\ s^{-1}$ was obtained from fitting of fluorescence transients generated by flash photolysis. The latter value is consistent with the fact that pK_a values of DMN (Grell et al., 1989) are intermediate between those of EGTA and fura-2. Our method for estimating the on rate of DMN by steady-state UV photolysis is similar to that of Zucker (1993), but we made a simplification such that we could neglect the influence of the fluorescent dye. Our value of $3.5 \times 10^7\ M^{-1}\ s^{-1}$ is also significantly higher than that of Zucker (1993), but somewhat lower than that of Ellis-Davies et al. (1996) and Escobar et al. (1995), which may be due to some unknown influences of the cytoplasm.

Mitochondrial Ca^{2+} uptake

Our study confirmed that, similar to the case of rat chromaffin cells (Herrington et al., 1996; Park et al., 1996), mitochondria play a fast and dominant role in the clearance of large $[Ca^{2+}]_i$ loads in bovine chromaffin cells. Moreover, we measured the kinetics of mitochondrial Ca^{2+} uptake in intact cells. The low affinity ($K_{1/2}$ = 36.7 μM, this study) and the cooperative Ca^{2+} binding of mitochondrial Ca^{2+} uniporter suggest that this uptake mechanism will be prominent only when $[Ca^{2+}]_i$ is greater than several μM. Actually, according to our values of V_{max} and $K_{1/2}$, when $[Ca^{2+}]_i$ rises to 5 μM, it will drop to its half-value, 2.5 μM, in 2.7 s. This is quite close to the reported $[Ca^{2+}]_i$ decay time constant of 3.2 s for large transients in rat chromaffin cells (Herrington et al., 1996). But when $[Ca^{2+}]_i$ is as low as 500 nM, the influx rate into mitochondria will be 928 nM/s, which is much smaller than other linear $[Ca^{2+}]_i$ clearance mechanisms, such as membrane Ca^{2+}-ATPase, Na^+-Ca^{2+} exchange, etc. This is consistent with the single exponential $[Ca^{2+}]_i$ decay with a time constant of 5–10 s observed for very small transients in bovine chromaffin cells (Neher and Augustine, 1992). In this study we showed that mitochondria in intact cells can sequester as much as 1 mM intracellular total Ca^{2+}, which, for a cell with a diameter of 15 μm, corresponds to 250 pA calcium influx through Ca^{2+} channels for 1 s. Thus mitochondria can act as a slow (lasting for several seconds) and high-capacity Ca^{2+} buffer during high Ca^{2+} loads, as seen in many cell types (see Nicholls and Åkermann, 1982; Gunter et al., 1994).

Because our cells were dialyzed by whole cell pipettes, the mitochondrial uptake mechanism may be affected by a loss of cytoplasmic ingredients and by deterioration of cellular functions. Furthermore, our pipette solutions were not specially designed to preserve energy metabolism and mitochondrial function, as done by Herrington et al. (1996). Thus our kinetic measurements may underestimate the physiological values. We did see some rundown of mitochondrial uptake in our experiments, but when we compared the V_{max} values measured at 5 min with those at 10 min after whole-cell recording, no significant differences could be observed.

We would like to thank Christian Heinemann for help in the construction of the setup, Drs. Corey Smith and Kevin Gillis for comments on the manuscript, and Frauke Friedlein and Michael Pilot for cell preparation.

This work was supported by the Behrens Weise Stiftung and by grants from the Deutsche Forschungsgemeinschaft (Ne 243/6-1) and the European Community (CHRX-CT940500) to EN.

REFERENCES

Ahmed, Z., and J. A. Connor. 1988. Calcium regulation by and buffer capacity of molluscan neurons during calcium transients. *Cell Calcium.* 9:57–69.

Al-Baldawi, N. F., and R. F. Abercrombie. 1995. Cytoplasmic calcium buffer capacity determined with Nitr-5 and DM-nitrophen. *Cell Calcium.* 17:409–421.

Baylor, S. M., and S. Hollingworth. 1988. Fura-2 calcium transients in frog skeletal muscle fibres. *J. Physiol. (Lond.).* 403:151–192.

Berlin, J. R., J. W. M. Bassani, and D. M. Bers. 1994. Intrinsic cytosolic calcium buffering properties of single rat cardiac myocytes. *Biopys. J.* 67:1775–1787

Blatter, L. A., and W. G. Wier. 1990. Intracellular diffusion, binding and compartmentalization of the fluorescent calcium indicators indo-1 and fura-2. *Biophys. J.* 58:1491–1499.

Brinley, J. F., T. Tiffert, A. Scarpa, and L. J. Mullins. 1977. Intracellular calcium buffering capacity in isolated squid axons. *J. Gen. Physiol.* 70:355–384.

Durussel, I., J. A. Rhyner, E. E. Strehler, and J. A. Cox. 1993. Cation binding and conformation of human calmodulin-like protein. *Biochemistry.* 32:6089–6094.

Ellis-Davies, G. C., J. H. Kaplan, and R. J. Barsotti. 1996. Laser photolysis of caged calcium: rate of calcium release by nitrophenyl-EGTA and DM-nitrophen. *Biophys. J.* 70:1006–1016.

Escobar, A. L., F. Cifuentes, and J. L. Vergara. 1995. Detection of Ca^{2+}-transients elicited by flash photolysis of DM-nitrophen with a fast calcium indicator. *FEBS Lett.* 364:335–338.

Falke, J. J., S. K. Drake, A. L. Hazard, and O. B. Peersen. 1994. Molecular tuning of ion binding to calcium signaling proteins. *Q. Rev. Biophys.* 27:219–290.

Fierro, L., and Llano, I. 1996. High endogenous calcium buffering in Purkinje cells from rat cerebellar slices. *J. Physiol. (Lond.).* 496: 617–625.

Gillis, K. D., R. Mößner, and E. Neher. 1996. Protein kinase C enhances exocytosis from chromaffin cells by increasing the size of the readily releasable pool of secretory granules. *Neuron.* 16:1209–1220.

Grell, E., E. Lewitzki, H. Ruff, E. Bamberg, G. C. R. Ellis-Davies, J. H. Kaplan, and P. De Weer. 1989. Caged Ca^{2+}: a new agent allowing liberation of free Ca^{2+} in biological systems by photolysis. *Cell. Mol. Biol.* 35:515–522.

Grynkiewiez, G., M. Poenie, and R. Y. Tsien. 1985. A new generation of Ca^{2+} indicators with greatly improved fluorescence properties. *J. Biol. Chem.* 260:3440–3450.

Gunter, T. E., K. K. Gunter, S. S. Sheu, and C. E. Gavin. 1994. Mitochondrial calcium transport: physiological and pathological relevance. *Am. J. Physiol.* 267(*Cell Physiol.* 36):C313–C339.

Hamill, O. P., A. Marty, E. Neher, B. Sakamnn, and F. J. Sigworth. 1981. Improved patch-clamp techniques for high resolution current recordings from cells and cell-free membrane patches. *Pflügers Arch. Eur. J. Physiol.* 391:85–100.

Heidelberger, R., C. Heinemann, E. Neher, and G. Matthews. 1994. Calcium dependence of the rate of exocytosis in a synaptic terminal. *Nature.* 371:513–515.

Heinemann, C., R. H. Chow, E. Neher, and R. S. Zucker. 1994. Kinetics of the secretory response in bovine chromaffin cells following flash photolysis of caged Ca^{2+}. *Biophys. J.* 67:2546–2557.

Herrington, J., Y. B. Park, D. F. Babcock, and B. Hille. 1996. Dominant role of mitochondria in clearance of large Ca^{2+} loads from rat adrenal chromaffin cells. *Neuron.* 16:219–228.

Hove-Madsen, L., and D. M. Bers. 1992. Indo-1 binding to protein in permeablized ventricular myocytes alters its spectral and Ca binding properties. *Biophys. J.* 63:89–97.

Jackson, A. P., M. P. Timmerman, C. R. Bagshaw, and C. C. Ashley. 1987. The kinetics of calcium binding to fura-2 and indo-1. *FEBS Lett.* 216:35–39.

Kao, J. P. Y., and R. Y. Tsien. 1988. Ca^{2+} binding kinetics of fura-2 and azo-1 from temperature-jump relaxation measurements. *Biophys. J.* 53: 635–639.

Kaplan, J. H., and G. C. R. Ellis-Davies. 1988. Photolabile chelators for rapid photolytic release of divalent cations. *Proc. Natl. Acad. Sci. USA.* 85:6571–6575.

Konishi, M., S. Hollingworth, A. B. Harkins, and S. M. Baylor. 1991. Myoplasmic calcium transients in intact frog skeletal muscle fibres monitored with the fluorescent indicator furaptra. *J. Gen. Physiol.* 97: 271–301.

Missiaen, L., F. Wuytack, L. Raeymaekers, H. D. Smedt, G. Droogmans, S. D. Jaegere, and R. Casteels. 1993. Ca^{2+} extrusion across plasma

membrane and Ca^{2+} uptake by intracellular stores. *In* Intracellular Messengers. C. W. Taylor, editor. Pergamon Press, Oxford. 347–405.

Müller, T. H., L. D. Partridge, and D. Swandulla. 1993. Calcium buffering in bursting *Helix* pacemaker neurons. *Pflügers Arch.* 425:499–505.

Neher, E. 1989. Combined fura-2 and patch clamp measurements in rat peritoneal mast cells. *In* Neuromuscular Junction. L. C. Sellin, R. Libelius, and S. Thesleff, editors. Elsevier Science. 65–76.

Neher, E., and G. J. Augustine. 1992. Calcium gradients and buffers in bovine chromaffin cells. *J. Physiol. (Lond.).* 450:273–301.

Neher, E., and R. S. Zucker. 1993. Multiple calcium-dependent processes related to secretion in bovine chromaffin cells. *Neuron.* 10:21–30.

Nicholls, D. G., and K. E. O. Åkerman. 1982. Mitochondrial calcium transport. *Biochim. Biophys. Acta.* 683:57–88.

Park, Y. B., J. Herrington, D. F. Babcock, and B. Hille. 1996. Ca^{2+} clearance mechanisms in isolated rat adrenal chromaffin cells. *J. Physiol. (Lond.).* 492:329–346

Rizzuto, R., A. W. M. Simpson, M. Brini, and T. Pozzan. 1992. Rapid changes of mitochondrial Ca^{2+} revealed by specifically targeted recombinant aequorin. *Nature.* 358:325–327.

Rutter, G. A., J. M. Theler, M. Murgia, C. B. Wollheim, T. Pozzan, and R. Rizzuto. 1993. Stimulated Ca^{2+} influx raises mitochondrial free [Ca^{2+} to supramicromolar levels in a pancreatic β-cell line. *J. Biol. Chem.* 268:22385–22390.

Tatsumi, H., and Y. Katayama. 1993. Regulation of the intracellular free calcium concentration in acutely dissociated neurons from rat nucleus basalis. *J. Physiol. (Lond.).* 464:165–181.

Thomas, P., J. G. Wong, A. K. Lee, and W. Almers. 1993. A low affinity Ca^{2+} receptor controls the final steps in peptide secretion from pituitary melanotrophs. *Neuron.* 11:93–104.

Weinstein, H., and E. L. Mehler. 1994. Ca^{2+}-binding and structural dynamics in the functions of calmodulin. *Annu. Rev. Physiol.* 56:213–236.

Zhou, Z., and E. Neher. 1993. Mobile and immobile calcium buffers in bovine adrenal chromaffin cells. *J. Physiol. (Lond.).* 469:245–273.

Zucker, R. S. 1992. Effects of photolabile calcium chelators on fluorescent calcium indicators. *Cell Calcium.* 13:29–40.

Zucker, R. S. 1993. The calcium concentration clamp: spikes and reversible pulses using the photolabile chelator DM-nitrophen. *Cell Calcium.* 14:87–100.